ACS APPLIED ENERGY MATERIALS

www.acsaem.org Article

Carbon Foams via Ring-Opening Metathesis Polymerization of Emulsion Templates: A Facile Method to Make Carbon Current Collectors for Battery Applications

Sebastijan Kovačič,* Bettina Schafzahl, Nadejda B. Matsko, Katharina Gruber, Martin Schmuck, Stefan Koller, Stefan A. Freunberger,* and Christian Slugovc*

Cite This: *ACS Appl. Energy Mater.* 2022, 5, 14381−14390 Read Online

ACCESS | Metrics & More | Article Recommendations | Supporting Information

ABSTRACT: Polydicyclopentadiene (pDCPD), a thermoset with excellent mechanical properties, has enormous potential as a lightweight, tough, and stable matrix material owing to its highly cross-linked macromolecular network. This work describes generating pDCPD-based foams and hierarchically porous carbons derived therefrom by combining ring-opening metathesis polymerization (ROMP) of DCPD, high internal phase emulsions (HIPEs) as structural templates, and subsequent carbonization. The structure and function of the carbon foams were characterized and discussed in detail using scanning electron, transmission electron, or atomic force microscopy (SEM, TEM, AFM), electron energy-loss spectroscopy (TEM-EELS), N_2 sorption, and analyses of electrical conductivity as well as mechanical properties. The resulting materials exhibited uniform, shape-retaining shrinkage of only ∼1/3 after carbonization. No structural failure was observed even when the pDCPD precursor foams were heated to 1400 °C. Instead, the high porosity, void size, and 3D interconnectivity were fully preserved, and the void diameters could be adjusted between 87 and 2.5 μm. Moreover, foams have a carbon content >97%, an electronic conductivity of up to 2800 $S \cdot m^{-1}$, a Young's modulus of up to 2.1 GPa, and a specific surface area of up to 1200 $m^2 \cdot g^{-1}$. Surprisingly, the pDCPD foams were carbonized into shapes other than monoliths, such as 10's of micron thick membranes or foamy coatings adhered to a metal foil or grid substrate. The latter coatings even adhere upon bending. Finally, as a use case, carbonized foams were applied as porous cathodes for Li−O_2 batteries where the foams show a favorable combination of porosity, active surface area, and pore size for outstanding capacity.

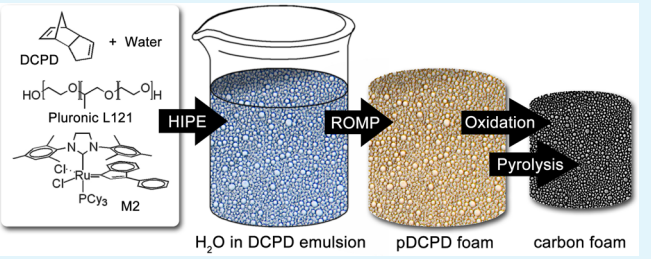

KEYWORDS: *emulsion templating, carbonization, ROMP, polyHIPEs, porous cathode*

INTRODUCTION

Ring-opening metathesis polymerization (ROMP) has become one of the most versatile polymerization techniques, finding application in many areas of polymer and materials research.[1−3] The ROMP of dicyclopentadiene (DCPD), a cheap byproduct in the C5 stream of naphtha crackers, is industrially relevant to fabricate, e.g., body panels for vehicles or cell covers for chloro-alkali plants, domestic wastewater treatment units, and large waste containers.[4−7] The thermoset poly(dicyclopentadiene) (pDCPD) is characterized by excellent mechanical properties with high toughness and rigidity and outstanding chemical resistance. The latter is ascribed to autoxidation of the surface of pDCPD.[8] Current research interests in pDCPD-based materials include polymerizable ferrofluids,[9] membranes for purification purposes,[10−12] nanoporous pDCPD,[13] pDCPD aerogels,[14,15] fibers made by electrospinning,[16] and emulsion-templated macroporous foams[17−23] or nanocomposites.[24−26] The macroporous foams are, in the context of this work, of particular interest. Generally, cellular polymer foams are usually prepared by chemical or physical foaming, whereby the cell sizes, morphologies, as well as the preparation of fully open-cell structures are difficult to control.[27] An alternative, offering a solution for that obstacle, is provided by the so-called emulsion-templating approach. High internal phase emulsions (HIPEs) are a special type of emulsions characterized by a droplet (internal) phase volume fraction exceeding 74.05% of the total emulsion volume.[28] Their structure consists of deformed (polyhedral) and/or polydispersed droplets separated by a thin film of the continuous phase (made up by monomers).[29] Polymerization of the continuous phase of a HIPE and removal of the droplets

Received: September 8, 2022
Accepted: October 16, 2022
Published: October 16, 2022

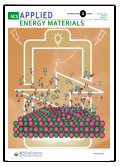

Table 1. Porosity and Void Sizes of Foams Prepared with Different Surfactant Amounts before and after Carbonization for 2 h at 900 °C

sample[a]	porosity before carbonization [%][b]	void sizes before carbonization [μm][c]	porosity after carbonization [%][d]	void sizes after carbonization [μm][e]
$pDCPD_{0.25}$	80	69 ± 53	82	87 ± 56
$pDCPD_1$	81	35 ± 23	82	33 ± 10
$pDCPD_3$	80	7.4 ± 5.5	84	10 ± 6
$pDCPD_5$	81	6.7 ± 2.6	85	6.4 ± 2.5
$pDCPD_7$	82	4.2 ± 2.4	85	4.3 ± 1.6
$pDCPD_{10}$	79	3.4 ± 1.2	84	2.5 ± 0.9

[a]Foams prepared with different surfactant loading given in the subscript in vol % with respect to DCPD. [b]Experimental porosity assessed with mercury porosimetry; see ref 18. [c]Diameter determined by SEM of broken samples; see ref 18. [d]Experimental porosity assessed with mercury porosimetry of samples carbonized at 900 °C (heating ramp 4 °C·min^{-1}, 2 h at 900 °C). [e]Diameter, determined by SEM of broken samples.

Table 2. Physical Properties of Carbon Foams Prepared from $pDCPD_7$ at Different Temperatures

Temp. [°C][a]	Porosity [%][c]	Void sizes [μm][d]	Window sizes [μm][d]	He dens. [g·cm^{-3}][e]	BET [m^2·g^{-1}][f]	BET [m^2·g^{-1}][g]	Electr. Cond.[S·m^{-1}][h]
500	79	4.2 ± 1.2	1.5 ± 0.9	1.38	2.50	497 ± 3	/
700	81	4.6 ± 1.6	2.1 ± 0.9	1.69	3.10	1182 ± 9	61 ± 4
900	85	4.3 ± 1.6	1.2 ± 0.6	2.09	22.6	626 ± 4	1150 ± 57
1100	85	4.5 ± 1.5	2.0 ± 1.6	2.07	10.1	946 ± 6	2410 ± 120
1400	81	3.9 ± 1.5	2.7 ± 0.9	1.68	4.10	313 ± 1	2790 ± 84
1400[b]	79	4.2 ± 1.4	1.2 ± 0.6	1.68	14.2	n.d.	2590 ± 90

[a]Carbonization temperature, heating ramp 4 °C·min^{-1}, 2 h at the given temperature. [b]Heating ramp 4 °C·min^{-1}, 8 h at 1400 °C. [c]Experimental porosity assessed by mercury porosimetry. [d]Diameter determined by SEM of broken samples. [e]Skeletal density determined by helium pycnometry. [f]Surface area determined by N_2-adsorption measurements (BET method). [g]Surface area after activation with CO_2 at the temperature listed in the first column as determined by N_2-adsorption measurements (BET method). [h]Electrical conductivity determined by a four-point method.

of the dispersed phase produce highly macroporous and permeable matrices (termed polyHIPEs). The resulting polyHIPE foams are typically made up of highly 3D-interconnected macropores (so-called voids, of typical diameters between 5 and 20 μm) and interconnecting pores (so-called windows; typically, between 0.1 and 2 μm). The materials are attractive for a wide range of applications including, e.g., filter membranes, adsorbents, supports for solid phase chemistry, ion exchange resins, scaffolds for tissue engineering, hybrid materials, and supports for CO_2 capture.[30]

Another use is to carbonize the polyHIPE foams, generating monolithic macroporous carbon scaffolds.[31,32] Carbon foams have been prepared from polyHIPE precursors based on poly(styrene) and poly(divinylbenzene),[33−36] poly(acrylonitrile),[37] furfural-phloroglucinol,[38] tannin,[39] Kraft black liquor,[40,41] 2,5-dihydroxy-1,4-benzoquinone, and urea[42] or resorcinol-formaldehyde resins.[43] In addition, the preparation of macroporous carbon composites through the carbonization of nanocomposite polyHIPE foams as templates has also been reported.[44−46] These HIPE-derived macroporous carbon foams have been used in various applications such as catalysis[47−49] and CO_2 capture,[46,50] or as carbon components in battery electrodes.[51−53]

To exploit the control over void and window size and porosity in the polyHIPEs in applications such as battery electrodes, the macroporous morphology of the polyHIPE must be preserved at the high temperatures required for carbonization. To avoid both severe shrinkage of the foam skeleton and collapse of the precursor morphology, a fixation step is required prior to carbonization. Processes and techniques disclosed so far to stabilize polyHIPE precursors before heating include sulfonation,[54] hyper-cross-linking,[55] Pickering-HIPE templating,[44,56] or oxidation in air at high temperature.[37,57] Although all of these techniques have been shown to be effective, incorporating heteroatoms into the precursor forms toxic gases during carbonization and, in the case of nanoparticles, increases the cost and complexity of the systems and presents additional challenges in purification and processing. Homogeneous fixation for homogeneous shrinking is challenging but required to avoid shape loss during carbonization.[37,54,55] Overall, a workflow for tunable foam morphology and simple, reliable, and nonhazardous fixation to obtain tailored carbon foams is still a challenge.

Herein, we show a ROMP-based strategy to prepare HIPE-derived carbon foams of various shapes, tunable pore sizes, high electronic conductivity, and high specific surface area, using the commodity monomer DCPD. The fixation step used here is very mild and homogeneous over the entire volume of the samples, resulting in relatively low and uniform shrinkage in all dimensions. This property represents a unique feature of this approach, which allows access to foams as monoliths, membranes, and coatings on substrates. Activation allows us to increase the active surface area to make them suitable for electrochemical applications, which we demonstrate with the Li−O_2 battery.[58−61]

EXPERIMENTAL SECTION

Materials. Dicyclopentadiene (DCPD, Aldrich), Pluronic L-121 (poly(ethylene glycol)-*block*-poly(propylene glycol)-*block*-poly(ethylene glycol), Aldrich), the initiator ((H$_2$IMes)(PCy$_3$)Cl$_2$Ru(3-phenyl-indenylid-1-ene) (M2, Umicore, H$_2$IMes = *N*,*N*-bis(mesityl) 4,5-dihydroimidazol-2-yl, PCy$_3$ = tricyclohexylphosphine)), and toluene (p.a. Aldrich) were used as received.

Synthetic Procedure. Preparation of Monolithic or Membrane HIPE-Derived Carbon Foams. The according amounts of monomer DCPD, Pluronic L121, (Table S1), and toluene (50 μL) were placed in a 3-neck round-bottomed flask equipped with a mechanical stirrer and a dropping funnel. The mixture was stirred at 400 rpm for 5 min, and upon continuous stirring deionized water was added dropwise at 25 °C over about 1 h. Afterward, the initiator M2 (1.3 mg, 0.0007 mmol with respect to DCPD) dissolved in toluene (0.25 mL) was

https://doi.org/10.1021/acsaem.2c02787
ACS Appl. Energy Mater. 2022, 5, 14381−14390

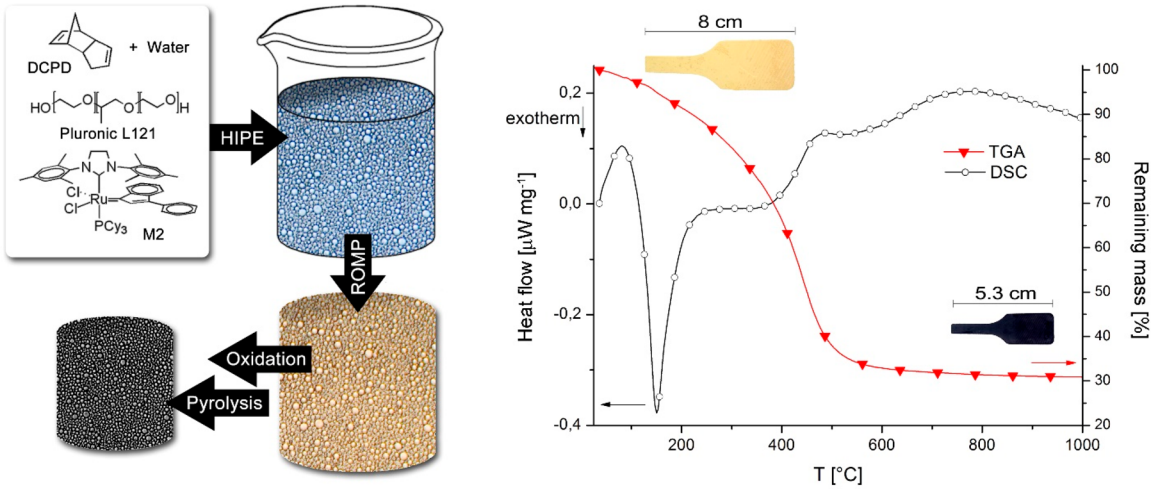

Figure 1. Left: preparation of the carbon foams. Right: combined TGA/DSC investigation of the carbonization process. Insets: photographs of a broken tensile test bar before (above) and after pyrolysis (below) indicating the sample's macroscopic shrinkage upon pyrolysis.

added, and the emulsion was stirred for a further 5 min. Subsequently, the emulsion was transferred to the appropriate mold (i.e., glass vials) for monoliths or casted onto the glass plates for membranes. The filled molds or casted glass plates were transferred into a preheated oven operating under air. Curing of the emulsions at 80 °C for 4 h resulted in the formation of white rigid monoliths in all cases. The specimens were purified by Soxhlet extraction with acetone for 24 h and subsequently dried in a desiccator under vacuum (10 mbar) until constant weight was reached. Such obtained specimens were placed in an oven operated in air and stored there for at least 5 days. Yet oxidized specimens were placed on a quartz boat in a quartz tube in the isothermal zone of a tubular furnace operated under argon. The samples were then heated to the temperature listed in Table 1 or with the heating ramp of 4 K/min.

Carbon Dioxide Activation. The CO_2 activations were performed using 500 mg of carbon foam for each batch. The raw material was placed in a quartz boat in a quartz tube in the isothermal zone of a tubular furnace and purged with flowing argon. The samples were then heated to the temperature as listed in Table 2 (temperatures given are of the furnace) with a heating rate of 4 K min^{-1} followed by subsequently changing the gas to CO_2 with a flow of 10 mL min^{-1} and annealing at the target temperature. Samples were cooled to room temperature under flowing argon.

Preparation of a Carbon-Foam-Coated Ni Substrate. DCPD-based HIPEs (HIPE preparation as described above) were cast onto nickel foils or a wire grid (purchased from Schlenk Metallfolien GmbH, 99.5%) without any surface pretreatment using a casting blade with a slit of 200 μm. Afterward the specimens were covered with a support lid in a way that direct contact of the lid with the casted HIPE was assured. Such prepared specimens were put into an oven operated at 80 °C for 2 h. Afterward the lid was removed and stored in an oven operated in air at 40 °C for 5 days in order to oxidize. Subsequent carbonization at 600 °C (heating ramp of 4 K/min) yielded a composite of the nickel substrate coated with macroporous carbon layers.

Electrochemical Methods. Cathodes were prepared by gently mixing hand-ground carbonized HIPEs with an isopropanol and polytetrafluoroethylene (PTFE, suspension in water, Aldrich) binder in a ratio of 9:1. This mixture was applied on an Al mesh current collector. The electrodes were washed with H_2O/acetone 1:1 and dried overnight under vacuum at 80 °C. Typical cathodes contained about 1−5 mg cm^{-2} of carbon. Equally, Ketjen Black or Super P (C-Energy) were used. Counter electrodes were made from $LiFePO_4$ (PI-Kem), Super P, and PTFE in a weight ratio of 8:1:1 and made analogously to the cathodes.

Characterization. TGA measurements were performed with a Netzsch Simultaneous Thermal Analyzer STA 449 F1 Jupiter (crucibles: aluminum from Netzsch). A nitrogen flow of 50 mL min^{-1} was used in combination with a protective flow of helium of 8 mL min^{-1}. The heating rate until a final temperature of 1100 °C was 10 K min^{-1}. Morphology was investigated using scanning electron microscopy (SEM). SEM images were taken on a Vega-3, Tescan microscope. Pieces of carbon foam (section of about 0.5 cm^2) were broken without using liquid nitrogen and mounted on a carbon tab, and SEM analysis has been conducted without prior gold sputtering as carbon foams themselves were conductive. For TEM analysis, samples were embedded in an Araldite/Epon embedding mixture, which was composed of 49% w/w Araldite/Epon stock solution, 49% w/w hardener DDSA (Fluka), and 2% w/w accelerator DMP-30 (Fluka). Infiltration was performed stepwise (impregnation at room temperature for 24 h and polymerization at 50 °C for 72 h). Embedded samples were sectioned using Leica Ultracut ultramicrotome to a thickness between 70 and 120 nm. All EFTEM experiments were acquired in TEM mode. For the calculation of elemental distribution images, a jump ratio method was used. The high-resolution transmission electron microscopy was done on a 200 kV field-emission gun microscope JEOL JEM 2100. Samples were dispersed in ethanol and placed on a copper holey carbon grid. Nitrogen adsorption measurements of carbon foams were performed on an IMI-HTP manometric gas analyzer (Hiden Isocehma). After degassing of the samples at 100 °C for 2 h in a dynamic vacuum, the skeletal sample density was measured using helium pycnometry (99.999% He; Messer) at 25 °C for the dead volume corrections. The specific surface areas were determined by the Brunauer−Emmett−Teller (BET) method in accordance with ISO 9277:2010(E) standards. The true porosity (experimental porosity) of each sample was determined by mercury intrusion porosimetry (Micromeritic WIN9400 Series).

RESULTS AND DISCUSSION

Synthesis and Morphological Properties. Following our established protocols[17−23] that allow pDCPD foams with different void and window sizes to be prepared by simply varying the amount of surfactant, HIPEs were prepared from water in DCPD (adjusting the phase ratio to ∼0.80) using Pluronic-L121 as the surfactant (Figure 1, left; amounts summarized in Table S1). Upon adding the initiator **M2**[62] and heating the emulsion for 2 h at 80 °C, monolithic macroporous foams with different void and window sizes were obtained (Table 1). The foams were dried and exposed to air at 40 °C for at least 5 days to oxidize the specimens.[17−23,63] The oxidation step is crucial for subsequent carbonization because

https://doi.org/10.1021/acsaem.2c02787
ACS Appl. Energy Mater. 2022, 5, 14381−14390

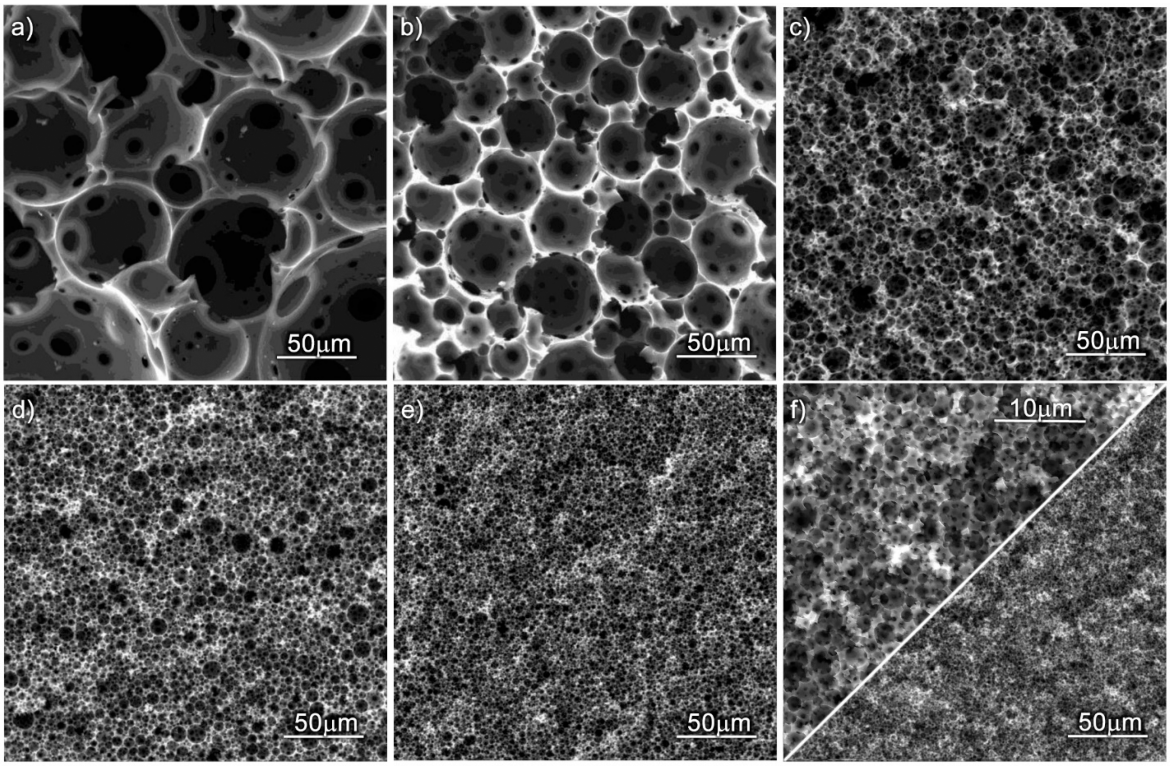

Figure 2. Morphology of the carbon foams obtained via pyrolyzing pDCPD foams with 80% nominal porosity prepared with (a) 0.25 vol %, (b) 1 vol %, (c) 3 vol %, (d) 5 vol %, (e) 7 vol %, and (f) 10 vol % of surfactant (shown above in a higher magnification).

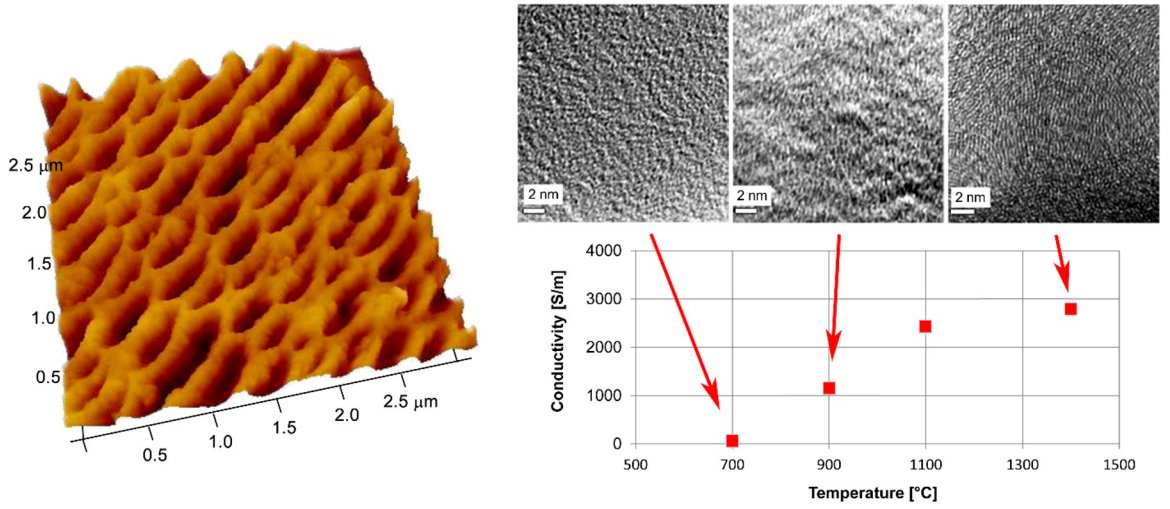

Figure 3. Left: AFM image of a carbonized foam wall. Right: HR-TEM images of the carbon morphology of the sample pyrolyzed at 700 °C (left), 900 °C (middle), and 1400 °C (right) and conductivity vs pyrolysis temperature (for error bars see Table 2).

it (additionally) cross-links the polymer backbone and fixes the macroporous morphology to maintain dimensional stability (unoxidized samples carbonize while losing the porous HIPE structure; see Figure S1). Complete oxidation resulted in a typical elemental composition of 62−65% C and 6−7% H (Table S2), which means that 28−32% oxygen was homogeneously incorporated into the foams (significantly more than the usual 6%),[37] due to a unique feature of pDCPD, the highly unsaturated backbone that results from metathesis polymerization.

Subsequently, the fully oxidized pDCPD foams were pyrolyzed at 900 °C under an inert argon atmosphere. The carbon foams retained their monolithic shape with a proportional shrinkage of about 33% in all dimensions and 67% of the size preserved (Figure 1). This is significantly less shrinkage than carbon foams fixed by other techniques, where shrinkage during carbonization is usually about 55%.[54−56] The excellent geometric stability of our carbon foams was further confirmed by the preserved macroporous morphology (Figure 2), which corresponds to that of the original pDCPD foam without void distortion and can be ascribed to the high tendency of the pDCPD precursor foam to oxidize. Carbonization resulted in a mass loss of 70 ± 3%, as indicated by TGA (Figure 1, right, and Figure S2).

https://doi.org/10.1021/acsaem.2c02787
ACS Appl. Energy Mater. 2022, 5, 14381−14390

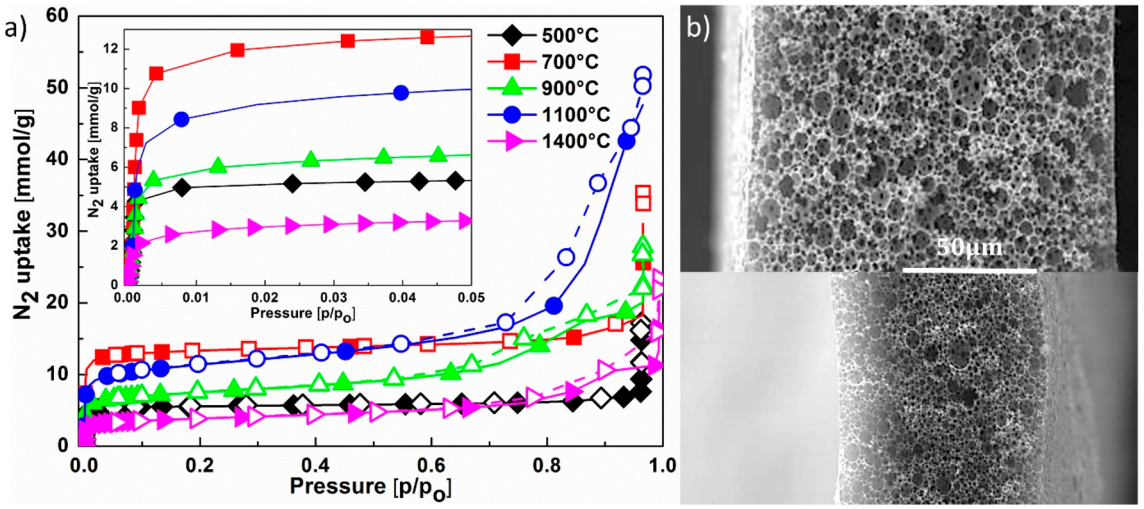

Figure 4. N_2 isotherms measured at 77 K of pDCPD carbon foams activated at different temperatures (a) and SEM picture of a pDCPD membrane of ~130 μm thickness (above) and (below) after pyrolysis in a thickness of 80 μm (b).

SEM shows that the characteristic morphologies of the HIPE-derived foams were preserved in the carbonized samples (Table 1, Figure 2, and Figures S3–6). Macroporous carbon foams with void diameters ranging from 2.5 ± 0.9 (HIPE prepared with 10 vol % surfactant) to 87 ± 56 μm (0.25 vol % surfactant used) were obtained. These values are comparable to the void diameters of the oxidized samples before pyrolysis (Table 1).[17−19] Considering that the specimens shrank to 67% of their initial size during carbonization, the unchanged void sizes are surprising at first glance. However, this phenomenon has already been described for other systems and is a common feature when carbonizing macroporous foams.[33,37,40] Thus, the ROMP-based system presented here allows the void sizes of the HIPE-derived carbon foam to be varied simply by varying the amount of surfactant used in the synthesis of the precursor. According to the elemental analysis, the carbon foams had a high carbon content of 96–98%. Other elements present were hydrogen (<1%) and oxygen (1.4–3.3%) (Table S2).

Next, the effect of carbonization temperature on the physical properties of carbon foams was investigated by pyrolyzing oxidized pDCPD foams prepared with 7 vol % of surfactant at 500, 700, 900, 1100, and 1400 °C for 2 h in an Ar atmosphere. These polymer foams, prepared from the HIPE precursor stabilized with 7% surfactant, have shown favorable properties, i.e., a good compromise between maximum porosity, void and window sizes, and good mechanical stability.[17−23] Regardless of the pyrolysis temperature, the morphology of the carbon foams was largely preserved after pyrolysis, and void sizes between 3.9 ± 1.5 μm and 4.6 ± 1.6 in diameter and window sizes between 1.2 ± 0.6 μm and 2.7 ± 0.9 μm in diameter (Table 2 and Figures S5 and S6) were obtained, as shown by the SEM analysis. Carbon foam skeletal densities were determined by helium pycnometry and increased from 1.380 g·cm^{-3} at 500 °C to 2.090 g·cm^{-3} at 900 °C. At higher pyrolysis temperatures, the skeletal density decreased again and reached 1.680 g·cm^{-3} at 1400 °C (Table 2). All skeletal densities observed here are lower than the density of graphite (2.25 g·cm^{-3}), suggesting a disordered carbon structure. Further information on the carbon foam structure at the nanoscale was obtained from high-resolution TEM micrographs (Figure 3, right), which show increasingly ordered carbon with increasing carbonization temperature. Electron energy loss spectroscopy (EELS) in the TEM mode confirmed this impression (Figure S7), showing the appearance of a feature at 6.5 eV energy loss corresponding to an orientation-dependent EELS excitation process of the π–π^* transition in the samples treated at higher temperatures. The low-loss spectra of the sample treated at 500 °C clearly indicate the presence of a fully amorphous carbon modification.[64,65] Similarly, the π^* peak at the C K-edge (at 284 eV energy loss) increases, indicating that the degree of graphitization increases with increasing pyrolysis temperature (Figure S6).[66]

This trend can be confirmed macroscopically by the increasing electronic conductivity of the samples with increasing pyrolysis temperature (Figure 3). Carbon foams treated at 500 °C are poor conductors, whereas a maximum conductivity of about 2800 S·m^{-1} was measured for the sample pyrolyzed at 1400 °C for 2 h (Figure 3, right; Tables 2 and S4). Finally, the mechanical properties of the samples prepared at 500 and 900 °C were determined by tensile tests (Figure S8, Table S5). The Young's moduli increased from 1.1 ± 0.2 GPa (pyrolysis at 500 °C) to 2.1 ± 0.3 GPa (900 °C). The samples fractured at a stress of 2.8 ± 0.2 MPa (500 °C) and 13.4 ± 0.6 MPa (900 °C) at an elongation of 0.3 ± 0.05% and 1.3 ± 0.3%, respectively. The samples produced at 1400 °C were too brittle to be measured.

Porosities. The carbon foams had porosity in the range of 79–85% as indicated by mercury porosimetry and a rather low specific surface area of 2.5–22.6 m^2·g^{-1} as determined by N_2 desorption measurements (BET method) (Table 2, Figure S9). The somewhat increased surface area of the samples pyrolyzed at 900 °C can be attributed to small macropores with diameters of about 350 nm within the polymer matrix, as shown by atomic force microscopy (AFM) studies (Figure 3, left, Figure S10 and TEM Figure S11). This pore formation can be explained by gas evolution during the carbonization process.[67] Additionally, subsequent surface activation of carbon foams with CO_2 greatly increases the pore volume specific surface area.[68] To significantly increase the surface area, the carbon foams were activated with CO_2 at the pyrolysis temperature (Table 2). N_2 physisorption isotherms showed a significant increase in N_2 uptake up to $0.1 p/p_0 \approx 0.1$ after activation of the samples with CO_2 (Figure 4a, inset), indicating the presence of micropores. The specific surface

https://doi.org/10.1021/acsaem.2c02787
ACS Appl. Energy Mater. 2022, 5, 14381−14390

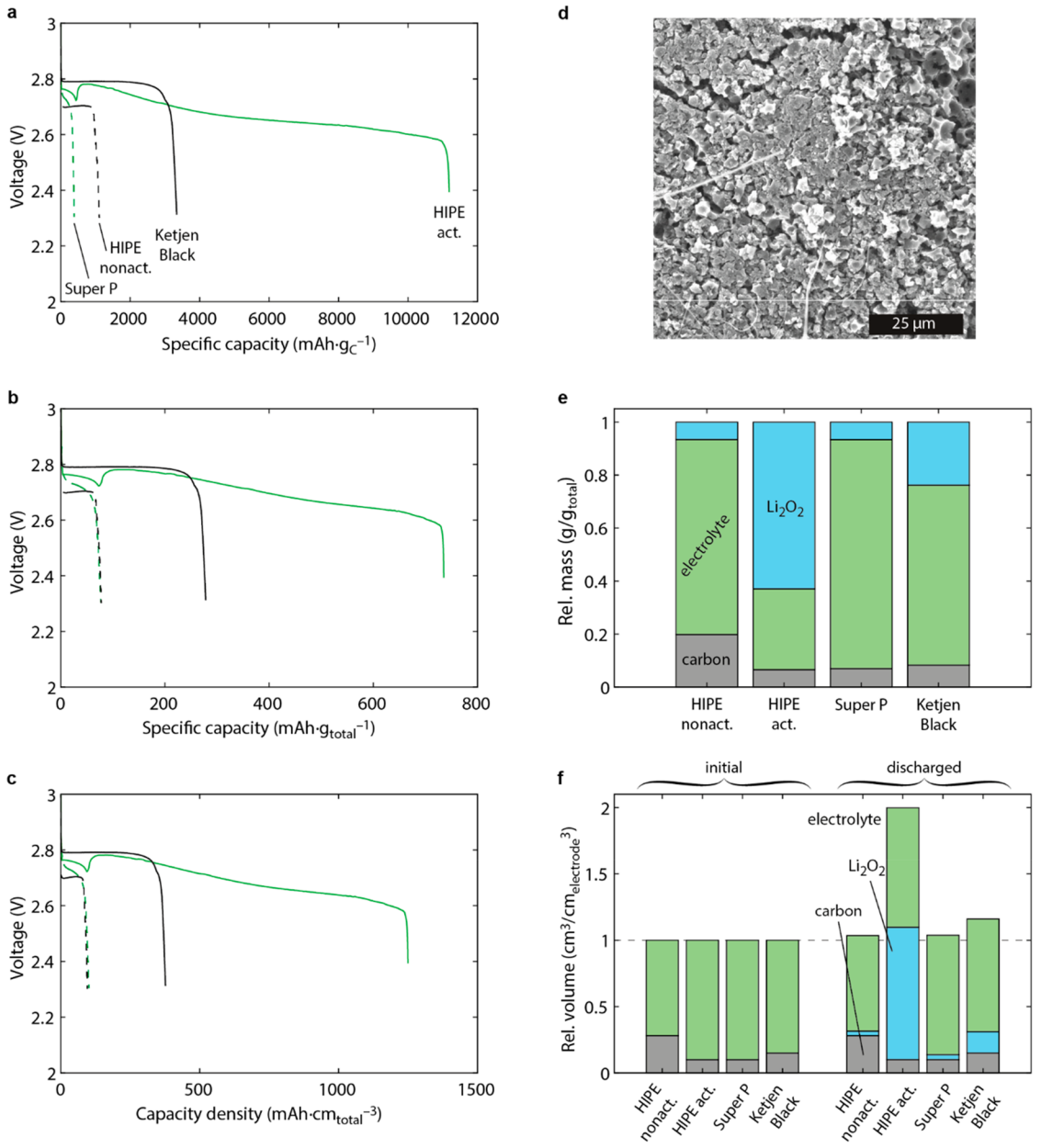

Figure 5. PolyHIPE-derived carbon foams for Li−O_2 battery cathodes. (a)−(c) Discharge voltage versus capacity for galvanostatic discharge of four different carbon materials with 0.1 M $LiNO_3$ in dimethylacetamide as electrolyte and a current of 70 mA g_C^{-1}. CO_2-activated and nonactivated carbonized HIPEs are compared with two commercially available carbon blacks, Ketjen Black (1200 m^2 g^{-1}) and SuperP (60 m^2 g^{-1}). The HIPEs were prepared with 7 vol % of surfactant and carbonized/activated at 1100 °C. Capacities are normalized with respect to (a) the carbon mass (mAh g_C^{-1}), (b) the total electrode weight including the formed Li_2O_2 and the electrolyte (mAh g_{total}^{-1}), and (c) the total volume of the electrode including the formed Li_2O_2 and the electrolyte (mAh cm_{total}^{-3}). (d) SEM image of the discharged activated HIPE electrode. (e) Relative masses at the end of discharge for carbon, electrolyte, and Li_2O_2. (f) Relative volumes at the end of discharge for carbon, electrolyte, and Li_2O_2 (right). Volumes are normalized with respect to the volume of the electrolyte-filled porous electrode before discharge (left). The Li_2O_2 in the pores displaces electrolyte beyond the initial electrolyte volume.

areas were calculated by the BET method (S_{BET}) and gave the highest S_{BET} value of 1182 $m^2 \cdot g^{-1}$ for the foam activated at 700 °C. The lowest surface area (313 $m^2 \cdot g^{-1}$) was found for the foam activated at 1400 °C. The samples activated at lower temperatures (i.e., 500 and 700 °C) exhibited a typical type I isotherm with only an additional steep increase at $p/p_0 \approx 1$, which can be attributed to the presence of macropores (Figure 4a). The isotherms of the samples activated at temperatures above 900 °C can be assigned to the type II isotherm, which has a hysteresis loop, indicating the presence of mesopores (Figure 4a and Figure S9). Mesoporosity was further rationalized by HR-TEM analysis, and mesopores with a diameter of 10−30 nm were observed (Figures S12 and S13).

Shaping. The results described so far were typically obtained with a monolithic cylindrical carbon specimen (diameter: 1.3 cm; height: 2.7 cm) or cuboidal specimen (for the four-point conductivity measurements; size: a = 20 cm; b = 1.5 cm; c = 0.5 cm). In addition, it is worth noting that other macroscopic shapes of carbon foams are easily accessible from the ROMP-based derivatives. To demonstrate this, carbon foam membranes with dimensions of 5 × 5 cm and a thickness of 80 µm were prepared (see Figures 4b and S14).

https://doi.org/10.1021/acsaem.2c02787
ACS Appl. Energy Mater. 2022, 5, 14381−14390

HIPE-Derived Carbon Foam as Li−O_2 Battery Cathodes. As a use case for the distinct properties of the HIPE-derived carbon foams, we demonstrate their use as porous cathodes for Li−O_2 batteries.

Their cycling mechanism causes them to require distinct combinations of porosity, active surface area, and pore size.[58−61] The cathode is in the charged state a porous carbon electrode that is filled with O_2-saturated liquid organic electrolyte in contact with an O_2 head space. As the battery discharges, dissolved O_2 is reduced at the pore surface to form solid Li_2O_2 particles. With a capacity of 1168 mAh per gram of Li_2O_2 (compared to ∼130−200 mAh g^{-1} for current intercalation cathode materials in Li ion batteries), Li−O_2 batteries could significantly outperform current batteries and have gained enormous research interest. Achievable capacity per electrode volume is determined by the initial porosity and the achievable degree of pore filling with Li_2O_2.[69] With common carbon materials, discharge quite typically ends at low degrees of pore filling as soon as the composite of carbon and Li_2O_2 becomes too tortuous for O_2 and ion transport. The latest understanding of the discharge mechanism states that Li_2O_2 morphologies with compact packing of several 100 nm particle sizes that pose the least impediment for O_2/ion transport require very low current densities w.r.t. the true pore surface of ≪0.1 μA cm_{real}^{-2} and the majority of the pore volumes stemming from pores a few μm in size.[61] While common activated carbons feature the required BET surface of around 1000 m^2 g^{-1}, they fail to provide the mentioned pore size.

Here we use the HIPE approach with subsequent activation to achieve such properties. We use the HIPE prepared with 7% surfactant and carbonized at 1100 °C in both the native and CO_2-activated form. This sample gives the best compromise w.r.t. surface area (946 $m^2 \cdot g^{-1}$) and conductivity (2410 $S \cdot m^{-1}$). With void and window sizes around 4 and 2 μm, respectively, much of the pore volume is made up by pores of this size. Figure 5 compares discharge curves of these two cathode materials with other commonly used carbon blacks, Super P (60 $m^2 \cdot g^{-1}$) and Ketjen Black (1200 $m^2 \cdot g^{-1}$). Figure 5a shows the common way of plotting capacity per gram of carbon. Expectedly, the nonactivated HIPE with only ∼10 $m^2 \cdot g^{-1}$ achieves only a few 100 mAh$\cdot g_C^{-1}$. We find capacities of ∼1000 and 3000 mAh$\cdot g_C^{-1}$ for Super P and Ketjen Black, respectively, in accordance with literature values.[61] The activated HIPE outperforms them ∼10-fold and 3-fold, respectively.

Plotting capacity per gram of carbon is common because metal−O_2 batteries are special in that the cathode in the charged state does not contain the redox material that could be taken as a reference for capacity. Thus, it is convenient to report capacities per weight of porous electrode, and additionally very larger numbers up to some 10,000 mAh$\cdot g_C^{-1}$ are often seen, which appears to compare favorably. However, this gives an unjust comparison to intercalation materials with ∼130−200 mAh$\cdot g^{-1}$. Figure 5b and c shows the relevant capacities w.r.t. total electrode mass and volume including the electrolyte and formed Li_2O_2. Associated relative masses and volumes of carbon, electrolyte, and Li_2O_2 are shown in Figure 5e and f. The results highlight that best exploiting the extraordinary theoretical capacity of Li_2O_2 requires the electrode pores being filled to the highest possible extent in order to maximize the active-to-inactive mass and volume ratio. The activated HIPE achieves this best among the materials shown, confirming its favorable combinations of porosity, active surface area, and pore size for Li−O_2 chemistry. Recharge of deeply discharged electrodes is hampered by electron transfer and generally accepted to require oxidation mediators with their own challenges.[70]

CONCLUSIONS

In summary, we have shown that emulsion-templated pDCPD foams are a versatile precursor to prepare porous carbons with tunable properties. The unique network structure of pDCPD, the highly unsaturated backbone that results from metathesis polymerization, allows for additional oxidative cross-linking that occurs when pDCPD ages in air at room temperature and is the key to preventing pDCPD foams from depolymerization and losing their porous properties during carbonization. While additional cross-linking is a common strategy to stiffen the polymer backbone prior to carbonization, herein it is achieved by mild and nonhazardous oxidation without the use of organic solvents, toxic reagents, or catalysts. The resulting porous carbon foams exhibit a 3D-interconnected microcellular morphology in the form of monoliths, membranes, or coatings, with pore sizes between 87 and 2.5 μm that can be tuned by the amount of surfactant in the HIPE. The carbon foams have excellent mechanical properties (Young's moduli of ∼2.1 GPa) and high electronic conductivity (up to 2800 $S \cdot m^{-1}$) and can be activated to get surface areas >1000 $m^2 \cdot g^{-1}$. Achievable shapes range from monoliths to membranes and coatings on flat metal and metal grid substrates. As a use case we apply them as porous cathodes for Li−O_2 batteries where activated HIPEs are shown to have a favorable combination of porosity, active surface area, and pore size for outstanding capacity. Overall, the ROMP process is shown as a very cheap and practical approach to make tailorable carbon foams. It can be more broadly applied to other ROMP-able monomers and opens up countless possibilities for future carbon foam research and applications.

ASSOCIATED CONTENT

Supporting Information

The Supporting Information is available free of charge at https://pubs.acs.org/doi/10.1021/acsaem.2c02787.

Details on the preparation, elemental analyses, SEM, AFM, TEM, and HR-TEM pictures, electron energy loss spectra, conductivity measurements, adsorption measurements, and tensile testing (PDF)

AUTHOR INFORMATION

Corresponding Authors

Sebastijan Kovačič − *Department of Inorganic Chemistry and Technology, National Institute of Chemistry, 1000 Ljubljana, Slovenia;* orcid.org/0000-0003-2664-9791; Email: sebastijan.kovacic@ki.si

Stefan A. Freunberger − *Institute of Science and Technology Austria (ISTA), 3400 Klosterneuburg, Austria;* orcid.org/0000-0003-2902-5319; Email: stefan.freunberger@ist.ac.at

Christian Slugovc − *Graz University of Technology, Institute of Chemistry and Technology of Materials, 8010 Graz, Austria*; Email: slugovc@tugraz.at

Authors

Bettina Schafzahl − *Graz University of Technology, Institute of Chemistry and Technology of Materials, 8010 Graz, Austria*

Nadejda B. Matsko − *Graz Centre for Electron Microscopy (FELMI-ZFE), 8010 Graz, Austria*

Katharina Gruber − *VARTA Innovation GmbH, 8010 Graz, Austria*

Martin Schmuck − *VARTA Innovation GmbH, 8010 Graz, Austria*

Stefan Koller − *VARTA Innovation GmbH, 8010 Graz, Austria*

Complete contact information is available at: https://pubs.acs.org/10.1021/acsaem.2c02787

Notes

The authors declare the following competing financial interest(s): Some of the authors are also authors of a patent (WO 2013178371 A1) on this topic.

■ ACKNOWLEDGMENTS

S.K. acknowledges the financial support from the Slovenian Research Agency (grants P1-0021, P2-0150). Support by Graz University of Technology (LP-03 − Porous Materials@Work) and from VARTA Innovation GmbH is kindly acknowledged. We thank Umicore for providing the initiator and Matjaž Mazaj (National Institute of Chemistry, Ljubljana) and Karel Jerabek (Czech Academy of Sciences) for measurements and fruitful discussions. S.A.F. is indebted to the Austrian Federal Ministry of Science, Research and Economy; the Austrian Research Promotion Agency (Grant No. 845364); and ISTA for support.

■ REFERENCES

(1) Bielawski, C. W.; Grubbs, R. H. Living ring-opening metathesis polymerization. *Prog. Polym. Sci.* **2007**, *32*, 1−29. d

(2) Leitgeb, A.; Wappel, J.; Slugovc, C. The ROMP toolbox upgraded. *Polymer* **2010**, *51*, 2927−2946.

(3) Slugovc, C. *Handbook of Metathesis*, 2nd ed.; Grubbs, R. H., Kosravi, E., Eds.; Wiley-VCH: Weinheim, 2015; Vol. *3*, p 1−16.

(4) Kovačič, S.; Slugovc, C. Ring-opening Metathesis Polymerisation derived poly(dicyclopentadiene) based materials. *Mater. Chem. Front.* **2020**, *4*, 2235−2255.

(5) Trimmer, M. S. *Handbook of Metathesis*; Wiley-VCH: Weinheim, 2003; Vol. *3*, p 407−414.

(6) Nickel, A.; Edgecombe, B. D. *Polymer Science: A Comprehensive Reference*; Elsevier: Amsterdam, 2012; Vol. *4*, p 749−759.

(7) Le Gac, P. Y.; Choqueuse, D.; Paris, M.; Recher, G.; Zimmer, C.; Melot, D. Durability of polydicyclopentadiene under high temperature, high pressure and seawater (offshore oil production conditions). *Polym. Degrad. Stab.* **2013**, *98*, 809−817.

(8) Mühlebach, A.; Van der Schaaf, P. A.; Hafner, A.; Setiabudi, F. Thermal stability and degradation of hydrocarbon metathesis polymers. *J. Mol. Catal. A: Chem.* **1998**, *132*, 181−188.

(9) Bian, P.; McCarthy, T. J. Polymerization of Monomer-Based Ferrofluids. *Langmuir* **2010**, *26*, 6145−6148.

(10) Perring, M.; Bowden, N. B. Assembly of Organic Monolayers on Polydicyclopentadiene. *Langmuir* **2008**, *24*, 10480−10487.

(11) Long, T. R.; Gupta, A.; Miller, A. L.; Rethwisch, D. G.; Bowden, N. B. Selective flux of organic liquids and solids using nanoporous membranes of polydicyclopentadiene. *J. Mater. Chem.* **2011**, *21*, 14265−14276.

(12) Gupta, A.; Bowden, N. B. Separation of cis-Fatty Acids from Saturated and trans-Fatty Acids by Nanoporous Polydicyclopentadiene Membranes. *ACS Appl. Mater. Interfaces* **2013**, *5*, 924−933.

(13) Amendt, M. A.; Roerdink, M.; Moench, S.; Phillip, W. A.; Cussler, E. L.; Hillmyer, M. A. Functionalized Nanoporous Membranes from Reactive Triblock Polymers. *Aust. J. Chem.* **2011**, *64*, 1074−1082.

(14) Mohite, D. P.; Mahadik-Khanolkar, S.; Luo, H.; Lu, H.; Sotiriou-Leventis, C.; Leventis, N. Polydicyclopentadiene aerogels grafted with PMMA: I. Molecular and interparticle crosslinking. *Soft Matter* **2013**, *9*, 1516−1530.

(15) Lenhardt, J. M.; Kim, S. H.; Nelson, A. J.; Singhal, P.; Baumann, T. F.; Satcher, J. H. Increasing the oxidative stability of poly(dicyclopentadiene) aerogels by hydrogenation. *Polymer* **2013**, *54*, 542−547.

(16) Bellan, L. M.; Coates, G. W.; Craighead, H. G. Poly(dicyclopentadiene) Submicron Fibers Produced by Electrospinning. *Macromol. Rapid Commun.* **2006**, *27*, 511−511.

(17) Kovačič, S.; Krajnc, P.; Slugovc, C. Inherently Reactive polyHIPE Material from Dicyclopentadiene. *Chem. Commun.* **2010**, *46*, 7504−7506.

(18) Kovačič, S.; Jeřabek, K.; Krajnc, P.; Slugovc, C. Ring Opening Metathesis Polymerisation of emulsion templated dicyclopentadiene giving open porous materials with excellent mechanical properties. *Polym. Chem.* **2012**, *3*, 325−328.

(19) Kovačič, S.; Matsko, N. B.; Jeřabek, K.; Krajnc, P.; Slugovc, C. On the Mechanical Properties of HIPE Templated Macroporous poly(Dicyclopentadiene) Prepared with Low Surfactant Amounts. *J. Mater. Chem. A* **2013**, *1*, 487−490.

(20) Kovačič, S.; Kren, H.; Krajnc, P.; Koller, S.; Slugovc, C. The use of an emulsion templated microcellular poly(dicyclopentadiene-co-norbornene) membrane as separator in lithium-ion batteries. *Macromol. Rapid Commun.* **2013**, *34*, 581−587.

(21) Knall, A.-C.; Kovačič, S.; Hollauf, M.; Reishofer, D. P.; Saf, R.; Slugovc, C. Inverse electron demand Diels-Alder (iEDDA) functionalisation of macroporous poly(dicyclopentadiene) foams. *Chem. Commun.* **2013**, *49*, 7325−7327.

(22) Kovačič, S.; Preishuber-Pflügl, F.; Pahovnik, D.; Žagar, E.; Slugovc, C. Covalent incorporation of the surfactant into high internal phase emulsion templated polymeric foams. *Chem. Commun.* **2015**, *51*, 7725−7728.

(23) Vakalopoulou, E.; Slugovc, C. The Effects of Enhancing the Crosslinking Degree in High Internal Phase Emulsion Templated Poly(dicyclopentadiene). *Macromol. Chem. Phys.* **2019**, *220*, 1900423.

(24) Kovačič, S.; Matsko, N. B.; Ferk, G.; Slugovc, C. Macroporous poly(dicyclopentadiene) γFe2O3/Fe3O4 nanocomposite foams by high internal phase emulsion templating. *J. Mater. Chem. A* **2013**, *1*, 7971−7978.

(25) Kovačič, S.; Mazaj, M.; Jeselnik, M.; Pahovnik, D.; Žagar, E.; Slugovc, C.; Zabukovec Logar, N. Synthesis and Catalytic Performance of Hierarchically Porous MIL-100(Fe)@polyHIPE Hybrid Membranes. *Macromol. Rapid Commun.* **2015**, *36*, 1605−1611.

(26) Kovačič, S.; Anžlovar, A.; Erjavec, B.; Kapun, G.; Matsko, N. B.; Zigon, M.; Zagar, E.; Pintar, A.; Slugovc, C. Macroporous ZnO Foams by High Internal Phase Emulsion Technique: Synthesis and Catalytic Activity. *ACS Appl. Mater. Interfaces* **2014**, *6*, 19075−19081.

(27) Lee, S.-T.; Ramesh, N. S. *Polymeric Foams: Mechanisms and Materials*, 2nd ed.; CRC Press: Boca Raton, 2009; pp 11−27.

(28) Zhang, H.; Cooper, A. I. Synthesis and applications of emulsion-templated porous materials. *Soft Matter* **2005**, *1*, 107−113.

(29) Cameron, N. R.; Sherrington, D. C. High internal phase emulsions (HIPEs) — Structure, properties and use in polymer preparation. *Adv. Polym. Sci.* **1996**, *126*, 163−214.

(30) Zhang, T.; Sanguramath, R. A.; Israel, S.; Silverstein, M. S. Emulsion Templating: Porous Polymers and Beyond. *Macromolecules* **2019**, *52*, 5445−5479.

(31) Edwards, C. J. C.; Hitchen, D. A.; Sharples, M. US Patent, US4775655, 1988.

(32) Thongprachan, N.; Yamamoto, T.; Chaichanawong, J.; Ohmori, T.; Endo, A. Preparation of macroporous carbon foam using emulsion templating method. *Adsorption* **2011**, *17*, 205−210.

(33) Wang, D.; Smith, N. L.; Budd, P. M. Polymerization and carbonization of high internal phase emulsions. *Polym. Int.* **2005**, *54*, 297−303.
(34) Woodward, R. T.; Fam, D. W. H.; Antony, D. B.; Hong, J.; McDonald, T. O.; Petit, C.; Shaffer, M. S. P.; Bismarck, A. Hierarchically porous carbon foams from pickering high internal phase emulsions. *Carbon* **2016**, *101*, 253−260.
(35) Hu, W.; Xie, F.; Li, Y.; Wu, Z.; Tian, K.; Wang, M.; Pan, L.; Li, L. Hierarchically Porous Carbon Derived from PolyHIPE for Supercapacitor and Deionization Applications. *Langmuir* **2017**, *33*, 13364−13375.
(36) Woodward, R. T.; Jobbe-Duval, A.; Marchesini, S.; Anthony, D. B.; Petit, C.; Bismarck, A. Hypercrosslinked polyHIPEs as precursors to designable, hierarchically porous carbon foams. *Polymer* **2017**, *115*, 146−153.
(37) Cohen, N.; Silverstein, M. S. Synthesis of emulsion-templated porous polyacrylonitrile and its pyrolysis to porous carbon monoliths. *Polymer* **2011**, *52*, 282−287.
(38) Brun, N.; Edembe, L.; Gounel, S.; Mano, N.; Titirici, M. M. Emulsion-Templated Macroporous Carbons Synthesized By Hydrothermal Carbonization and their Application for the Enzymatic Oxidation of Glucose. *ChemSusChem* **2013**, *6*, 701−710.
(39) Szczurek, A.; Fierro, V.; Pizzi, A.; Celzard, A. Emulsion-templated porous carbon monoliths derived from tannins. *Carbon* **2014**, *74*, 352−362.
(40) Foulet, A.; Birot, M.; Backov, R.; Sonnemann, G.; Deleuze, H. Preparation of hierarchical porous carbonaceous foams from Kraft black liquor. *Mater. Today Commun.* **2016**, *7*, 108−116.
(41) Jalalian, M.; Jiang, Q.; Birot, M.; Deleuze, H.; Woodward, R. T.; Bismarck, A. Frothed black liquor as a renewable cost effective precursor to low-density lignin and carbon foams. *React. Funct. Polym.* **2018**, *132*, 145−151.
(42) Kapilov-Buchman, K.; Portal, L.; Zhang, Y.; Fechler, N.; Antonietti, M.; Silverstein, M. S. Hierarchically porous carbons from an emulsion-templated, urea-based deep eutectic. *J. Mater. Chem. A* **2017**, *5*, 16376−16385.
(43) Gross, A. F.; Nowak, A. P. Hierarchical Carbon Foams with Independently Tunable Mesopore and Macropore Size Distributions. *Langmuir* **2010**, *26*, 11378−11383.
(44) Woodward, R. T.; Fam, D. W. H.; Anthony, D. B.; Hong, J.; McDonald, T. O.; Petit, C.; Shaffer, M. S. P.; Bismarck, A. Hierarchically porous carbon foams from pickering high internal phase emulsions. *Carbon* **2016**, *101*, 253−260.
(45) Woodward, R. T.; Markoulidis, F.; De Luca, F.; Anthony, D. B.; Malko, D.; McDonald, T. O.; Shaffer, M. S. P.; Bismarck, A. Carbon foams from emulsion-templated reduced graphene oxide polymer composites: electrodes for supercapacitor devices. *J. Mater. Chem. A* **2018**, *6*, 1840−1849.
(46) Mazaj, M.; Bjelica, M.; Žagar, E.; Zabukovec Logar, N.; Kovačič, S. Zeolite Nanocrystals Embedded in Microcellular Carbon Foam as a High-Performance CO_2 Capture Adsorbent with Energy-Saving Regeneration Properties. *ChemSusChem* **2020**, *13*, 2089−2097.
(47) Yi, F.; Gao, Y.; Li, H.; Yi, L.; Chen, D.; Lu, S. Nitrogen- and oxygen-codoped porous carbonaceous foam templated from high internal emulsion as PtRu catalyst support for direct methanol fuel cell. *Electrochim. Acta* **2016**, *211*, 768−776.
(48) Zeng, M.; Wang, Y.; Liu, Q.; Yuan, X.; Feng, R.; Yang, Z.; Qi, C. N-doped mesoporous carbons supported palladium catalysts prepared from chitosan/silica/palladium gel beads. *Int. J. Biol. Macromol.* **2016**, *89*, 449−455.
(49) Zhang, Y.; Shen, Y.; Chen, Y.; Yan, Y.; Pan, J.; Xiong, Q.; Shi, W.; Yu, L. Hierarchically carbonaceous catalyst with Brønsted−Lewis acid sites prepared through Pickering HIPEs templating for biomass energy conversation. *Chem. Eng. J.* **2016**, *294*, 222−235.
(50) Huang, K.; Chai, S.-H.; Mayes, R. T.; Tan, S.; Jones, C. W.; Dai, S. Significantly increasing porosity of mesoporous carbon by $NaNH_2$ activation for enhanced CO_2 adsorption. *Microporous Mesoporous Mater.* **2016**, *230*, 100−108.
(51) Brun, N.; Prabaharan, S. R. S.; Morcrette, M.; Sanchez, C.; Pécastaings, G.; Derré, A.; Soum, A.; Deleuze, H.; Birot, M.; Backov, R. Hard Macrocellular Silica Si(HIPE) Foams Templating Micro/Macroporous Carbonaceous Monoliths: Applications as Lithium Ion Battery Negative Electrodes and Electrochemical Capacitors. *Adv. Funct. Mater.* **2009**, *19*, 3136−3145.
(52) Brun, N.; Prabaharan, S. R. S.; Morcrette, M.; Deleuze, H.; Birot, M.; Babot, O.; Achard, M.-F.; Surcin, C.; Backov, R. Design of Hierarchical Porous Carbonaceous Foams from a Dual-Template Approach and Their Use as Electrochemical Capacitor and Li Ion Battery Negative Electrodes. *J. Phys. Chem. C* **2012**, *116*, 1408−1421.
(53) Roberts, A. D.; Li, X.; Zhang, H. Porous carbon spheres and monoliths: morphology control, pore size tuning and their applications as Li-ion battery anode materials. *Chem. Soc. Rev.* **2014**, *43*, 4341−4356.
(54) Asfaw, H. D.; Younesi, R.; Valvo, M.; Maibach, J.; Ångström, J.; Tai, C.-W.; Bacsik, Z.; Sahlberg, M.; Nyholm, L.; Edström, P. K. Boosting the thermal stability of emulsion−templated polymers via sulfonation: an efficient synthetic route to hierarchically porous carbon foams. *ChemistrySelect* **2016**, *1*, 784−792.
(55) Israel, S.; Levin, M.; Oliel, S.; Mayer, D.; Lerner, I.; Silverstein, M. S. Hierarchical Porosity in Emulsion-Templated, Porogen-Containing Interpenetrating Polymer Networks: Hyper-Cross-Linking and Carbonization. *Macromolecules* **2022**, *55* (6), 1992−2002.
(56) Ungureanu, S.; Birot, M.; Deleuze, H.; Schmitt, V.; Mano, N.; Backov, R. Triple hierarchical micro-meso-macroporous carbonaceous foams bearing highly monodisperse macroporosity. *Carbon* **2015**, *91*, 311−320.
(57) Even, W. R.; Gregory, D. P. Emulsion-Derived Foams: Preparation, Properties, and Application. *MRS Bull.* **1994**, *19*, 29−33.
(58) Wang, Y.; Lu, Y.-R.; Dong, C.-L.; Lu, Y.-C. Critical Factors Controlling Superoxide Reactions in Lithium−Oxygen Batteries. *ACS Energy Lett.* **2020**, *5*, 1355−1363.
(59) Lim, H.-D.; Lee, B.; Bae, Y.; Park, H.; Ko, Y.; Kim, H.; Kim, J.; Kang, K. Reaction chemistry in rechargeable Li-O2 batteries. *Chem. Soc. Rev.* **2017**, *46*, 2873−2888.
(60) Mahne, N.; Fontaine, O.; Thotiyl, M. O.; Wilkening, M.; Freunberger, S. A. Mechanism and performance of lithium-oxygen batteries - a perspective. *Chem. Sci.* **2017**, *8*, 6716−6729.
(61) Prehal, C.; Samojlov, A.; Nachtnebel, M.; Lovicar, L.; Kriechbaum, M.; Amenitsch, H.; Freunberger, S. A. In situ small-angle X-ray scattering reveals solution phase discharge of $Li-O_2$ batteries with weakly solvating electrolytes. *Proc. Natl. Acad. Sci. U.S.A.* **2021**, *118*, e2021893118.
(62) Leitgeb, A.; Wappel, J.; Urbina-Blanco, C. A.; Strasser, S.; Wappl, C.; Cazin, C. S. J.; Slugovc, C. Two commercially available initiators for the retarded ring-opening metathesis polymerization of dicyclopentadiene. *Monatsh. Chem.* **2014**, *145*, 1513−1517.
(63) Vakalopoulou, E.; Borisov, S.; Slugovc, C. Fast Oxygen Scavenging of Macroporous Poly(Norbornadiene) Prepared by Ring-Opening Metathesis Polymerization. *Macromol. Rapid Commun.* **2020**, *41*, 1900581.
(64) Monthioux, M.; Soutric, F.; Serin, V. Recurrent correlation between the electron energy loss spectra and mechanical properties for carbon fibers. *Carbon* **1997**, *35*, 1660−1664.
(65) Daniels, H. R.; Brydson, R.; Brown, A.; Rand, B. Quantitative valence plasmon mapping in the TEM: viewing physical properties at the nanoscale. *Ultramicroscopy* **2003**, *96*, 547−558.
(66) Orientation-dependent EELS excitation processes such as the ($\pi-\pi^*$) low-loss feature (at 6.5 eV energy loss) and the π^* peak at the C−K-edge (at 284 eV energy loss) display an orientation dependence, which is too strong to use these peaks to quantify the degree of carbonization.
(67) Zhang, Z.; Brydson, R.; Aslam, Z.; Reddy, S.; Brown, A.; Westwood, A.; Rand, B. Investigating the structure of non-graphitising carbons using electron energy loss spectroscopy in the transmission electron microscope. *Carbon* **2011**, *49*, 5049−5063.

https://doi.org/10.1021/acsaem.2c02787
ACS Appl. Energy Mater. 2022, 5, 14381−14390

(68) Borchardt, L.; Oschatz, M.; Kaskel, S. Tailoring porosity in carbon materials for supercapacitor applications. *Mater. Horiz.* **2014**, *1*, 157−168.
(69) Freunberger, S. A. True performance metrics in beyond-intercalation batteries. *Nat. Energy* **2017**, *2*, 17091.
(70) Petit, Y. K.; Mourad, E.; Prehal, C.; Leypold, C.; Windischbacher, A.; Mijailovic, D.; Slugovc, C.; Borisov, S. M.; Zojer, E.; Brutti, S.; Fontaine, O.; Freunberger, S. A. Mechanism of Mediated Alkali Peroxide Oxidation and Triplet Versus Singlet Oxygen Formation. *Nat. Chem.* **2021**, *13*, 465−471.

https://doi.org/10.1021/acsaem.2c02787
ACS Appl. Energy Mater. 2022, 5, 14381−14390